Appl. Phys. A 60, 137–142 (1995)

Applied Physics A Materials Science & Processing

Femtosecond time-resolved reflection second-harmonic generation on polycrystalline copper

J. Hohlfeld[1], D. Grosenick[2], U. Conrad[1], E. Matthias[1]

[1] Fachbereich Physik, Freie Universität Berlin, Arnimallee 14, D-14195 Berlin, Germany (Fax: + 49-30/838-6059)
[2] Max-Born-Institut, Rudower Chaussee 6, D-12474 Berlin, Germany

Received: 20 June 1994 / Accepted: 28 September 1994

Abstract. Optical Second-Harmonic Generation (SHG) in reflection from a polycrystalline copper surface in air was studied using femtosecond time-resolved pump and probe measurements at $\lambda = 625$ nm. The observed time dependence of second-harmonic yield from the probe beam demonstrates, that SHG is a very sensitive technique for measuring transient electron temperatures of metals even when these are covered by an oxide layer. For polycrystalline copper, an electron–phonon energy transfer time of 2 ps was observed, corresponding to a coupling constant of 3.75×10^{17} W/m^3 K at average lattice temperatures of about 500 K. The analysis of experimental data indicates that the time dependence of SHG is governed by the linear dielectric function ε which, in turn, is affected by the electron temperature. There is no evidence for a temperature dependence of the nonlinear susceptibility $\chi^{(2)}$.

PACS: 142.65.Ky; 63.20.Kr; 78.47. + p

The behaviour of transient stages in metals far from equilibrium has been the subject of theoretical investigations for four decades [1, 2]. By photon absorption from ultrashort pulses, it should be possible to heat the conduction electrons on a time scale shorter than the electron–phonon energy relaxation time up to several thousand K while the lattice remains relatively cold. The non-equilibrium temperature difference results from the fact that the electronic heat capacity is about one to two orders of magnitude smaller than the lattice heat capacity. The subsequent equilibration of the electron gas and the lattice is determined by electron–electron scattering, electron–phonon scattering, and heat transport. The knowledge of these relaxation processes supplies transport properties like electrical and thermal conductivity, for example, allowing to check theories about superconductivity [3] or the determination of damage thresholds of metals [4].

The development of stable ultrashort laser-pulse sources has triggered many experimental investigations on this subject, using Transient Thermo Reflectance Spectroscopy (TTRS) [5–10], Transient Thermo Transmittance Spectroscopy (TTTS) [11], multiphoton photoemission [12–14] and reflectance detection of surface-plasmon resonances [15, 16]. The thermalization of the electron gas [13, 14], the equilibration of electron gas and lattice [5–11], as well as heat transport by hot electrons [8] were examined. Apart from substantial objections [13–17] concerning data interpretation by the widely used two-temperature model [2], non-equilibrium stages of metals are well understood.

In noble metals, TTRS uses time-resolved differential reflectivity measurements to monitor electronic interband transitions from d bands to conduction-band energies near the Fermi level [5, 9]. Electron heating broadens the Fermi-Dirac distribution leading to an increased electron density above the Fermi energy and a corresponding decrease below. These changes in electronic occupancy are the dominant contributions to electron-temperature-induced variations of the dielectric function for photon energies near the interband-transition threshold which is monitored by TTRS.

The main scope of our investigations was to examine the influence of non-equilibrium stages of a metal on optical SHG on metal surfaces, extending traditional TTRS to nonlinear optics. We work on the assumption that these experiments can even be carried out in air, and that a thin oxide layer will not significantly affect either the SHG or the electron–phonon dynamics in the near-surface region.

SHG in reflection is most sensitively affected by two parameters: the second-order susceptibility $\chi^{(2)}$ and the linear dielectric function ε. $\chi^{(2)}$ describes the intrinsic ability of a sample to generate second-harmonic radiation, whereas the fraction of the incident field at ω that will be the source for SHG is determined by $\varepsilon(\omega)$. The ratio of reflected vs absorbed SH is then governed by $\varepsilon(2\omega)$. When,

Paper presented at the 129th WE-Heraeus-Seminar on "Surface Studies by Nonlinear Laser Spectroscopies", Kassel, Germany, May 30 to June 1, 1994

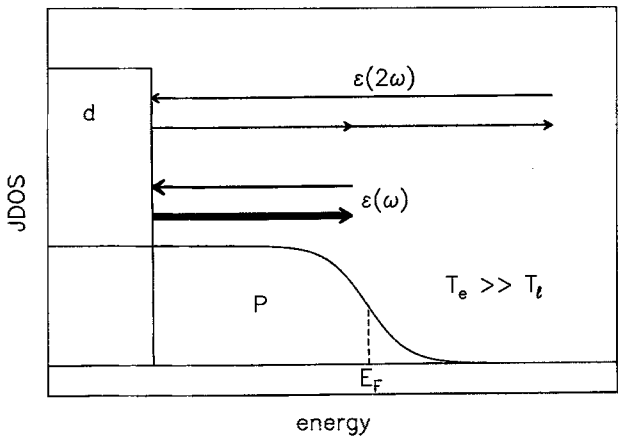

Fig. 1. Schematic representation of Joined Density Of States (JDOS) for Cu at $T_e \gg T_l$. The decreased electronic occupancy below the Fermi energy due to the temperature broadening of the Fermi-Dirac distribution results primarily in an increase in linear absorption which is proportional to the imaginary part of the dielectric function $\varepsilon_2(\omega)$

for SHG, the intermediate state at $\hbar\omega$ is nearly resonant with the Fermi energy, the temperature broadening of the Fermi-Dirac distribution will strongly affect the SH yield. This is illustrated in Fig. 1. In general, a reduction in electronic occupancy below the Fermi energy causes enhancement of linear absorption and of the nonlinear susceptibility $\chi^{(2)}$ [18, 19] for photon energies smaller than the interband-transition threshold. There is, however, experimental evidence that the behaviour of the linear response will dominate SHG changes when ω or 2ω is in resonance with electronic transitions. Li et al. [20] could explain their wavelength-dependent measurements of SHG on the Ag(1 1 1) surface taking only the variation of the dielectric function $\varepsilon(2\omega)$ into account. In this paper, we present further evidence that temperature-induced changes of $\chi^{(2)}$ are indeed overruled by the dielectric function, entering through the Fresnel factors.

We selected copper where the distance between d-band and Fermi level best matched the wavelength of our laser, and extended the ideas of Li et al. [20] to interpret time-resolved SH measurements that we carried out on polycrystalline Cu in terms of changes of $\varepsilon(\omega)$ and $\varepsilon(2\omega)$ due to a transient electron temperature.

1 Theoretical model

The interpretation of the experimental data is based on a combination of three different models, to describe the three main aspects of our experiment, namely SHG, electron-temperature-induced changes of the dielectric function, and the coupling of non-equilibrium electron temperatures to the lattice.

1.1 SHG *in reflection*

For calculating the SHG in reflection from a copper surface, we followed a phenomenological model presented by Sipe et al. [21]. They have shown that the P-polarized SH field $E_p^{2\omega}$, generated on isotropic surfaces by p-polarized fundamental radiation E_0 and an angle of incidence Θ, might be expressed in the dipole approximation as:

$$E_p^{2\omega} = \frac{2i\omega}{c}|E_0|^2\,\delta z[A_p F_c \chi_{xzx}^{(2)} 2 f_c f_s + A_p N^2 F_s(\chi_{zxx}^{(2)} f_c^2 + \chi_{zzz}^{(2)} f_s^2)]t_p^2. \quad (1)$$

Here, δz denotes an effective interaction length of a few monolayers, and the abbreviations used in (1) are given by:

$$f_s = \frac{\sin\Theta}{n(\omega)},\quad f_c = \sqrt{1-f_s^2},\quad t_p = \frac{2\cos\Theta}{n(\omega)\cos\Theta + f_c},$$

$$t_s = \frac{2\cos\Theta}{\cos\Theta + n(\omega) f_c},\quad A_{p/s} = \frac{2\pi T_{p/s}}{\cos\Theta},\quad N = n(2\omega). \quad (2)$$

Equivalent expressions for $F_{s/c}$ and $T_{s/c}$ with N are used, where lower-case (capital) letters denote quantities of the fundamental (second harmonic).

We expect that the temperature dependence of SH yield is transmitted by the factors defined in (2), since they all depend on the linear dielectric function in form of the index of refraction $n(T_e, \omega) = [\varepsilon(T_e, \omega)]^{1/2}$. Further, we notice that the contributions of the three independent tensor elements $\chi_{zzz}^{(2)}$, $\chi_{zxx}^{(2)}$, and $\chi_{xzx}^{(2)}$ to SHG become distinguishable, because they are combined with different factors of (2), leading to different temperature dependences.

1.2 Temperature dependence of the dielectric function

According to a refined version of the model derived by Jah and Warke [22] and Rustagi [23] the electron temperature dependence of the dielectric function $\varepsilon(T_e, \omega) = \varepsilon_1(T_e, \omega) + i\varepsilon_2(T_e, \omega)$ is given by:

$$\varepsilon(T_e, \omega) = 1 - \frac{\omega_p^2}{\omega(\omega + i/\tau)} + 3\frac{\omega_p^2}{\omega^2}\frac{f_{dp}}{k_F(T_e)\,E_F(T_e)} \times \int_0^{\sqrt[3]{2}k_F} \left(\frac{z_1^2}{k^2 - z_1^2} - \frac{z_1'^2}{k^2 + z_1'^2} - \frac{2z_0^2}{k^2 - z_0^2}\right) \times E_{pk}[1 - F(T_e, k)]\,dk, \quad (3)$$

with the abbreviations:

$$z_n^2 = \frac{2m}{\hbar^2}(n\hbar\omega + in\hbar\omega_c - \Delta),$$

$$z'^2_n = \frac{2m}{\hbar^2}(n\hbar\omega + in\hbar\omega_c + \Delta),$$

$$E_{pk} = \Delta + \frac{k^2\hbar^2}{2m},$$

$$E_F(T_e) = E_{F0}\left[1 - \frac{\pi^2}{12}\left(\frac{kT_e}{E_{F0}}\right)^2\right], \quad (4)$$

$$\tau = \tau_0\left(\frac{E_F}{\hbar\omega - E_F}\right)^2.$$

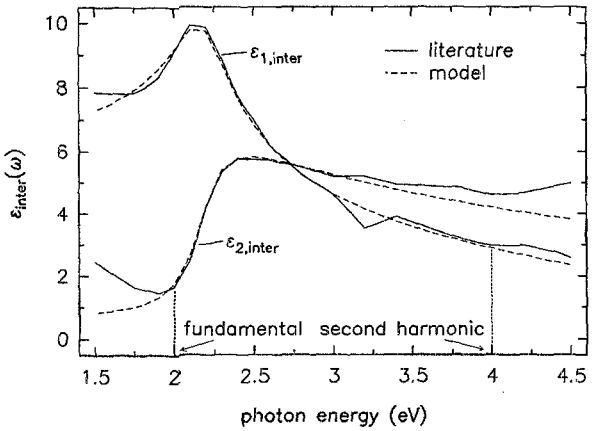

Fig. 2. Calculated frequency dependence of the real ε_1 and imaginary ε_2 part of the interband contribution of the dielectric function $\varepsilon_{inter}(\omega)$ in comparison with literature data [32]

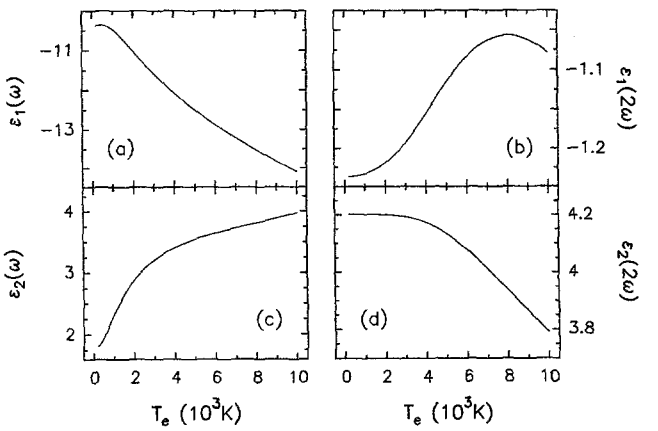

Fig. 3a–d. Calculated electron-temperature dependence of the real (**a**, **b**) and imaginary (**c**, **d**) parts of $\varepsilon(\omega)$ and $\varepsilon(2\omega)$

Here, Δ is the energy gap between d- and p-band at the center of the Brillouin zone, f_{dp} the oscillator strength for $d \rightarrow p$ transitions, ω_c the electron collision frequency, and ω_p the plasma frequency. The first two terms on the right-hand side of (3) describe the plasma or intraband contribution $\varepsilon_{intra}(\omega)$. The last term is the interband part $\varepsilon_{inter}(\omega)$, the wavelength dependence of which is shown in Fig. 2.

The refinements introduced by us are the temperature dependence of the Fermi energy [24] and the energy-dependent relaxation time τ [25] of the electron gas. Besides this, we accounted for contributions of other transitions [26, 27] by adding a constant value of 3.1 to the real part of the dielectric function.

We used $E_{F0} = 7.0$ eV [28, 29], $\omega_p = 9.06$ eV [30, 31] and $\tau_0 = 3.5 \times 10^{-14}$ s [27] from the literature to calculate the frequency dependence of the dielectric function at a fixed temperature of 297 K. By fitting our results to existing experimental data of [32], we obtained the following quantities: $\Delta = -4.82$ eV, $\omega_c = 0.11$ eV, and $f_{dp} = 0.28$. The quality of this fit is shown in Fig. 2. Inserting these parameters into (3) and (4), we determined the electron–temperature dependence of the linear dielectric function for the fixed photon energies of the fundamental, 2 eV, and the second harmonic, 4 eV. The results are displayed in Fig. 3.

Figure 4 shows the temperature dependence of the reflectivity R and the extinction coefficient α which are related to ε by:

$$R(T_e, \omega) = \frac{2A + A^2 + \varepsilon_2(T_e, \omega)^2 - \sqrt{2^3 A^3}}{2A + A^2 + \varepsilon_2(T_e, \omega)^2 + \sqrt{2^3 A^3}}, \tag{5}$$

$$\alpha(T_e, \omega) = \frac{2\omega}{c} \frac{\varepsilon_2(T_e, \omega)}{\sqrt{2A}}. \tag{6}$$

The abbreviation A used in (5) and (6) is defined as:

$$A = \varepsilon_1(T_e, \omega) + \sqrt{\varepsilon_1(T_e, \omega)^2 + \varepsilon_2(T_e, \omega)^2}.$$

To complete our theoretical model, we have to determine the time dependence of the electron temperature, which is discussed in the next section.

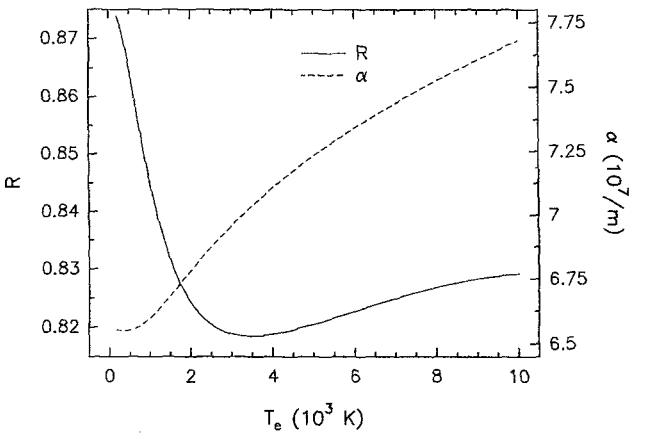

Fig. 4. Theoretical dependence of the linear reflectivity R and the linear extinction coefficient α of Cu on electron temperature T_e

1.3 The heat-flow model

As the electron temperature T_e is defined by the best fit of the electron-energy distribution to the Fermi-Dirac distribution, we have to examine the time dependence of the electron-energy distribution originating from the laser pulses. In general, this time dependence is dominated by three processes, namely, electron–electron and electron–phonon scattering, as well as energy diffusion. When the thermalization of the electron gas due to electron–electron scattering is faster than the other processes, T_e is well defined. Thus, the equilibration of electron gas and lattice is determined by the electron–phonon-coupling constant g and may be modelled by the two-temperature model presented by Anisimov et al. [2]:

$$C_e(T_e)\frac{\partial T_e}{\partial t} = K\frac{\partial^2 T_e}{\partial z^2} - g(T_e - T_l) + S(z, t),$$

$$C_l\frac{\partial T_l}{\partial t} = g(T_e - T_l), \tag{7}$$

$$S(z, t) = [1 - R(T_e)]\alpha\, e^{-\alpha z} I(t).$$

In (7), K denotes the thermal conductivity, C_l and $C_e(T_e)$ the lattice and electronic heat capacities, respectively. The

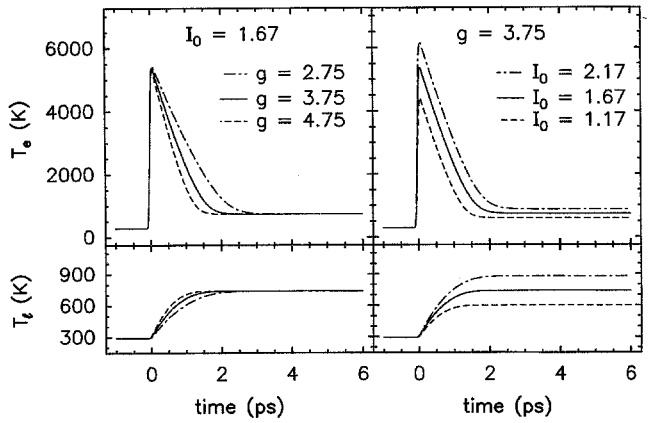

Fig. 5. Numerical modelling of the time evolution of the electron (*upper frames*) and lattice (*lower frames*) temperatures for the three electron–phonon coupling constants g (*left*) and three intensities of incident radiation I_0 (*right*). The values of g and I_0 are given in units of 10^{17} W/m^3 K and 10^{15} W/m^2, respectively

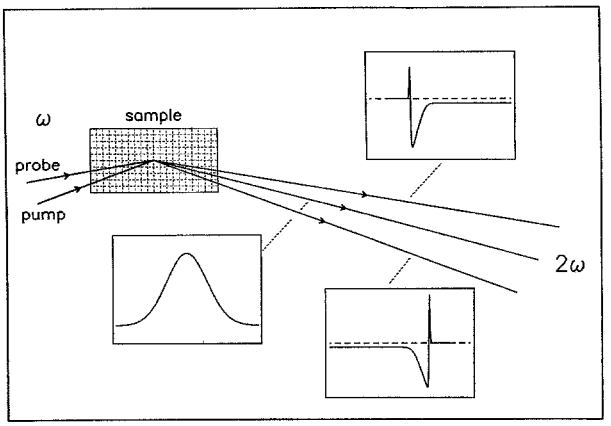

Fig. 6. Schematics of incident and reflected laser-beam directions and (*in the insets*) observed shapes of the SHG signals

values for copper are: $C_l = 3.43 \times 10^6$ J/m^3 K, and $C_e(T_e) = (96.6 \times T_e)$ J/m^3 K [33]. The source term $S(z, t)$ is given by the absorbed fraction of the incoming light intensity $I(t)$. For the reason of its small diffusivity, resulting from the large lattice heat capacity, heat diffusion in the lattice is neglected.

Investigations of the thermalization of electrons [13, 14] and the effect of a non-thermal electron distribution on the electron–phonon energy relaxation process in noble metals [15] have shown that the two-temperature model is only valid if the condition $kT_{e,\max} \approx \hbar\omega$ is fulfilled. The fluences used in our experiment were sufficiently high to satisfy this condition. The heat capacity of the electrons is assumed to increase linearly with temperature. At high temperatures, where it will reach the lattice value, the energy diffusion of the electrons may also be neglected.

The set of coupled, nonlinear differential equations (7), simplified in this manner, was numerically solved for the surface ($z = 0$), considering that the time dependence of the source term is given by a combined action of the pump and probe pulses. The simulation proceeded in the following way: We varied the delay time in discrete steps of 10 fs and calculated the relevant electron and lattice temperatures for each delay. We assumed given values for the reflectivity R and the extinction coefficient α for one time interval to calculate T_e, which was used to generate new values of R and α, for the next time interval, and so on. The time dependence of the calculated electron and lattice temperatures for three values of the electron–phonon coupling constants g and three different intensities of the incident radiation I_0 are shown in Fig. 5. It is obvious that the different influence of g and I_0 on T_e allows an unambiguous determination of g from the fits to experimental data.

2 Experiment

The laser system used for our investigations consists of a colliding-pulse mode-locked dye laser, producing laser pulses of 65 fs duration at a wavelength of 625 nm (2 eV) and a repetition rate of 76 MHz. These pulses were amplified up to 20 μJ in three amplification stages pumped by an excimer laser at 308 nm and repetition rates of a few Hz.

Pump and probe beams were generated by a 1:1 beam splitter and focused to about 250 μm diameter on the sample at an incident angle of 45°. The probe pulses passed through a half-wave plate, a glan prism and were delayed with respect to the pump pulses by a computer-controlled delay stage with 0.1 μm step size. In the actual experiment, a typical step size of 3 μm, corresponding to 10 fs, was used. Radiation at the SH frequency along the beam path arising from optical elements and from the excimer laser was suppressed by a 2 mm OG2 Schott filter. This filter is the entrance of a dark box, which included all following elements up to a monochromator, shielding them from any radiation of the excimer laser. These elements were the sample, two 2 mm UG5 Schott filters to suppress most of the fundamental radiation, and the polarization analyzer. The beam configuration for observing SHG is shown in Fig. 6. By turning the sample, SHG could be observed in either one of the three outgoing directions.

A plane-parallel mirror on a translation stage in front of the sample was used to send the beams into a BBO crystal to obtain the reference autocorrelation of the pulses. This allowed the control of the pulse length and the determination of zero delay between pump and probe beams.

The measurements were carried out with a polished polycrystalline copper sample in air. SH radiation generated at the sample surface was detected by a photomultiplier and amplified by a boxcar integrator. The generated analog signal was digitized and stored for every shot by a computer. Since the laser-pulse energies showed strong fluctuations, a reference signal proportional to the pulse energy was measured and all SH signals were sorted according to distinct energy intervals defined by this reference. The sorting intervals were chosen to limit the pulse-energy variations to five percent. We used this procedure instead of the usual normalization of the SH signal to the square of the reference signal, because the decrease of SH yield with electron temperature and energy-dependent variations of the beam profile caused significant deviations from this law.

3 Results and discussion

The search for SH radiation with different polarization combinations of the fundamental and the second harmonic, such as p-in, P/S-out, and s-in, P/S-out, was only successful for p-in and P-out, even when we increased the sensitivity of our detection about two orders of magnitude. In combination with symmetry considerations [34], this indicates that non-local bulk contributions are negligible and that the only significant element of $\chi^{(2)}$, describing the local surface response (1), is $\chi^{(2)}_{zzz}$.

As indicated in Fig. 6, SH radiation was detected in the directions of the specular reflexes of pump and probe beam as well as in the middle between them. The delay-dependent SH radiation in the center direction corresponds to the autocorrelation of the pulses which is broadened by the timing mismatch of ≈ 75 fs, resulting from the angle of $\approx 5°$ between the pump and probe beams and the beam diameter of 250 μm, but narrowed by electron heating. Figure 7 shows the autocorrelation data from the copper surface in comparison with the reference autocorrelation. The coincidence of the maxima demonstrates that both may serve for the calibration of zero delay.

A typical measurement of the time-resolved change of the SH yield normalized to the signal obtained in absence of the pump beam is shown in Fig. 8 together with theoretical curves calculated with our model. Each point displayed in the figure represents the average value of about thousand laser shots. The residual scatter of our data is primarily caused by variations of the beam profiles. Since pump and probe beams were p-polarized, we observe a peak of ≈ 70 fs FWHM around zero delay. This coherence peak is followed by a steep decrease of the SH yield on a time scale of the pulse duration down to a minimum value. This rapid decline of SHG is consistent with the fast reduction of electronic occupancy below the Fermi energy due to photoexcitation and electron–electron scattering. Due to the much higher cross section for linear absorption, emptied states below the Fermi energy absorb more

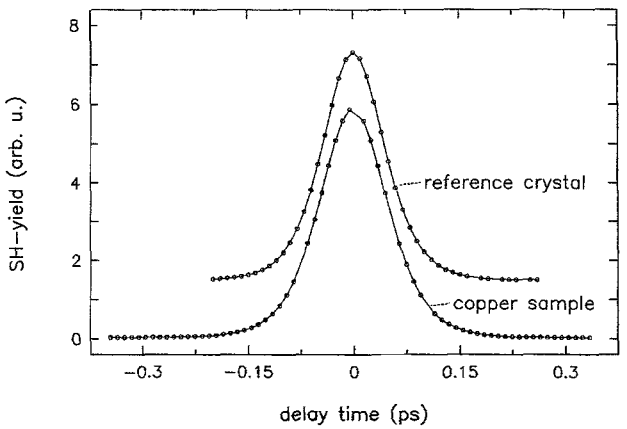

Fig. 7. Non-collinear second-order autocorrelation from the Cu sample (115 fs FWHM) and from the reference crystal (95 fs FWHM). The width of the autocorrelation from the Cu surface is broadened by geometry and narrowed by electron heating. The maxima of both signals define zero delay

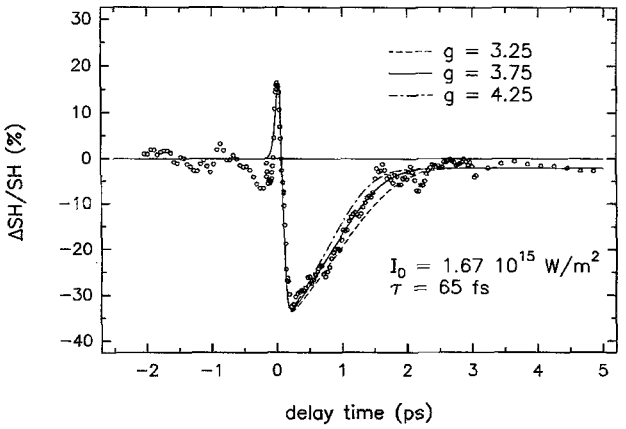

Fig. 8. Measured change of the P-polarized second-harmonic yield, normalized to the SH yield of the probe beam only, ΔSH/SH, as a function of delay time between the p-polarized pump and probe pulses. The values of g are given in units of 10^{17} W/m^3 K

single photons thereby reducing SHG. For larger delays between pump and probe pulses, the electron–lattice relaxation starts to cool the electron temperature, narrowing the Fermi distribution. Thus, the subsequent increase to a final level which is somewhat lower than the initial one is determined by electron–phonon scattering and lasts about ≈ 2 ps. The final level results from residual lattice heating which cools in tens of picoseconds via diffusion.

Modelling the experimental data, we considered the coherence peak, not discussed here, just as an additative sech^2-peak of arbitrary height and 65 fs duration. The calculations were first performed for different values of the three independent tensor elements, but the boundary condition that the lattice temperature has to stay below the melting point could only be fulfilled if $\chi^{(2)}_{zzz} \geqslant 750\, \chi^{(2)}_{xzx}$ and $\chi^{(2)}_{zzz} \geqslant 5000\, \chi^{(2)}_{zxx}$. This result is very consistent with our polarization-dependent measurements. We therefore neglected $\chi^{(2)}_{zxx}$ and $\chi^{(2)}_{xzx}$ in the simulations.

The used models described in Sect. 1 find there justification in the good agreement between all features of the experimental data and the theoretical curves. This agreement indicates that any influence of the oxide layer or metal/oxide interface is negligible. The oxide layer – which is a semiconductor – is not expected to posses an electron–phonon relaxation close to that of copper metal and should, therefore, not interfere with the pump–probe data in Fig. 8. The influence of the interface presents a more subtle problem, in particular, since the SHG response is dominated by $\chi^{(2)}_{zzz}$. However, experimental evidence was provided by Liu et al. [10] that metal/metal interfaces (Co/Cu and Ag/Cu) have little effect on the electron–lattice relaxation time. A metal/oxide interface should have even less, if any. Secondly, the electronic structure of the interface differs from that of the metal and should therefore evade our model description. The very fact that our model correctly reproduces the breakdown of SHG caused by electron heating and broadening of the Fermi edge for the wavelength chosen (Fig. 8), makes us confident that the SHG indeed probes the near-surface range of copper metal.

The best fit to our data corresponds to an electron–phonon constant of $g = 3.75 \times 10^{17}$ W/m^3 K with an accuracy of about fifteen percent. Taking into account that g is not a constant but temperature dependent as well, our results are in good agreement with those obtained by linear techniques are [6, 11]. The corresponding calculated temperature rise of the lattice of ≈ 820 K would also be expected on the basis of the lattice specific heat, the illuminated volume $V \simeq 10^{-15}$ m^3, and the absorbed laser-pulse energy $E_{abs} \simeq 2.8$ μJ.

4 Concluding remarks

We have shown that femtosecond time-resolved SHG is a sensitive technique for measuring transient electron temperatures of metals even under normal conditions. This allows the determination of electron–phonon relaxation times in the near-surface region. For polycrystalline copper, a relaxation time of 2 ps was found, corresponding to an electron–phonon coupling constant of 3.75×10^{17} W/m^3 K at average lattice temperatures of about 500 K. The model-independent relaxation time agrees well with results given in the literature [10, 11], suggesting that the metal-oxide interface does not significantly influence the electron–phonon relaxation near the copper surface. We found strong evidence that the observed temperature dependence of SHG at a polycrystalline copper surface and fundamental photon energies of 2 eV is caused by the linear dielectric function $\varepsilon(\omega)$. For interpreting the data, there is no need to invoke a temperature dependence of the nonlinear susceptibility $\chi^{(2)}$. Advantages of time-resolved SHG measurements compared to linear techniques [9, 11, 16] are the surface sensitivity and the order of magnitude larger effects.

Further measurements employing traditional TTRS and time-resolved SHG under the same conditions are desirable, since comparison of the two results should be able to uncover possible differences between electron–phonon interactions at surfaces and in the bulk.

Acknowledgements. This work was supported by the Deutsche Forschungs Gemeinschaft, Sonderfor schungsbereich 290. The collaboration of the Max-Born-Institute is gratefully acknowledged. One of us (JH) would like to thank Dr. Frank Noack and Dr. Frank Seifert for many helpful discussions.

References

1. M.I. Kaganov, I.M. Lifshitz, L.V. Tanatarov: Sov. Phys.-JETP **4**, 173 (1957)
2. S.I. Anisimov, B.L. Kapeliovich, T.L. Perel'man: Sov. Phys.-JETP **39**, 375 (1975)
3. P.B. Allen: Phys. Rev. Lett. **59**, 1460 (1987)
4. P.B. Corkum, F. Brunel, N.K. Sherman, T. Srinivasan-Rao: Phys. Rev. Lett. **61**, 2886 (1988)
5. G.L. Eesley: Phys. Rev. Lett. **51**, 2140 (1983)
6. G.L. Eesley: Phys. Rev. B **33**, 2144 (1986)
7. C.A. Paddock, G.L. Eesley: J. Appl. Phys. **60**, 285 (1986)
8. S.D. Brorson, J.G. Fujimoto, E.P. Ippen: Phys. Rev. Lett. **59**, 1962 (1987)
9. R.W. Schoenlein, W.Z. Lin, J.G. Fujimoto, G.L. Eesley: Phys. Rev. Lett. **58**, 1680 (1987)
10. D. Liu, P. He, D.R. Alexander: Appl. Phys. Lett. **62**, 249 (1992)
11. H.E. Elsayed-Ali, T.B. Norris, M.A. Pessot, G.A. Mourou: Phys. Rev. Lett. **58**, 1212 (1987)
12. J.G. Fujimoto, J.M. Liu, E.P. Ippen, N. Bloembergen: Phys. Rev. Lett. **53**, 1837 (1984)
13. W.S. Fann, R. Storz, H.W.K. Tom. J. Bokor: Phys. Rev. Lett. **68**, 2834 (1992)
14. W.S. Fann, R. Storz, H.W.K. Tom, J. Bokor: Phys. Rev. B **46**, 13592 (1992)
15. R.H.M. Groeneveld, R. Sprik, A. Lagendijk: Phys. Rev. B **45**, 5079 (1992)
16. R.H.M. Groeneveld, R. Sprik, A. Lagendijk: Phys. Rev. Lett. **64**, 784 (1990)
17. A. Lörincz, Z. Bozóki, A. Miklós: J. Appl. Phys. **70**, 941 (1991)
18. L.E. Urbach, K.L. Percival, J.M. Hicks, E.W. Plummer, H.L. Dai: Phys. Rev. B **45**, 3769 (1962)
19. T.F. Heinz, F.J. Himpsel, E. Palange, E. Burstein: Phys. Rev. Lett. **63**, 644 (1989)
20. C.M. Li, L.E. Urbach, H.L. Dai: Phys. Rev. B **49**, 2104 (1994)
21. J.E. Sipe, D.J. Moss, H.M. van Driel: Phys. Rev. B **35**, 1129 (1987)
22. S.S. Jah, C.S. Warke: Phys. Rev. **153**, 751 (1967)
23. K.C. Rustagi: Il Nuovo Cimento *LIII*, 346 (1968)
24. W. Greiner, L. Neise, H. Stöcker: *Thermodynamik und Statistische Mechanik* (Deutsch, Thun 1987)
25. D. Pines, P. Nozières: *The Theory of Quantum Liquids* (Benjamin, Menlo Park 1966)
26. R. Rosei, D.W. Lynch: Phys. Rev. B **5**, 3883 (1972)
27. H. Ehrenreich, H.R. Philipp: Phys. Rev. **128**, 1622 (1962)
28. H. Ibach, H. Lüth: *Festkörperphysik*, 3rd edn. (Springer, Berlin, Heidelberg 1990)
29. C. Kittel: *Einführung in die Festkörperphysik* (Oldenbourg, München 1976)
30. C.Y. Fong, M.L. Cohen, R.R.L. Zucca, J. Stokes, Y.R. Shen: Phys. Rev. Lett. **25**, 1486 (1970)
31. P.B. Johnson, R.W. Christy: Phys. Rev. B **6**, 4370 (1972)
32. E.D. Palik (ed.): *Handbook of Optical Constants of Solids*, Part I (Academic, Orlando 1985)
33. D.E. Gray (ed.): *American Institute of Physics Handbook* (McGraw-Hill, New York 1972)
34. P.N. Butcher, D. Cotter: *The Elements of Nonlinear Optics* (Cambridge Univ. Press, Cambridge 1990)